Topology optimization of surface-enhanced Raman scattering substrates

Ying Pan, Rasmus E. Christiansen, Jérôme Michon, et al.

View Online   Export Citation   CrossMark

ARTICLES YOU MAY BE INTERESTED IN

Topology optimization of surface-enhanced Raman scattering substrates

View Online   Export Citation   CrossMark

Ying Pan,[1,2] (iD) Rasmus E. Christiansen,[3,4,5,a)] (iD) Jérôme Michon,[1,2] Juejun Hu,[1,2] (iD) and Steven G. Johnson[3] (iD)

AFFILIATIONS

[1]Department of Materials Science and Engineering, Massachusetts Institute of Technology, Cambridge, Massachusetts 02139, USA
[2]Materials Research Laboratory, Massachusetts Institute of Technology, Cambridge, Massachusetts 02139, USA
[3]Department of Mathematics, Massachusetts Institute of Technology, Cambridge, Massachusetts 02139, USA
[4]Department of Mechanical Engineering, Technical University of Denmark, Nils Koppels Allé, Building 404, 2800 Kongens Lyngby, Denmark
[5]NanoPhoton—Center for Nanophotonics, Technical University of Denmark, Ørsteds Plads 345A, DK-2800 Kgs. Lyngby, Denmark

[a)]Author to whom correspondence should be addressed: raelch@mek.dtu.dk

ABSTRACT

Surface-enhanced Raman spectroscopy is a powerful and versatile sensing method with a detection limit down to the single molecule level, given sufficiently high signal enhancement. In this article, we demonstrate how topology optimization (TopOpt) can be used for designing surface enhanced Raman scattering (SERS) substrates adhering to realistic fabrication constraints. As an example, we experimentally demonstrated a SERS enhancement factor of 5×10^4 for the $604 \, cm^{-1}$ Raman line of rhodamine 6G using metal nanostructures with a critical dimension of 20 nm. We then show that, by relaxing the fabrication minimum-feature-size constraint, TopOpt may be used to design SERS substrates with orders of magnitude larger enhancement factor. The results validate topology optimization as an effective method for engineering optimized SERS nanostructures adhering to fabrication limitations.

Published under an exclusive license by AIP Publishing. https://doi.org/10.1063/5.0055148

We demonstrate the power of topology optimization (TopOpt)[1–3] as a tool for inverse design of direct-lithography manufacturable periodic surface enhanced Raman scattering (SERS) metasurfaces[4–11] through design, fabrication, and experimental validation. We show that imposing fabrication limitations incurred when using electron-beam-lithography (EBL) directly as part of the TopOpt procedure (an out-of-plane sidewall slant angle and minimum-feature-size of design members) ensures a close correspondence between the design blueprint and the fabricated structure, without the need for post-lithography processing. By relaxing the minimum-feature-size constraint, we demonstrate numerically that combined bowtie and horn-like nanostructure emerges, which exhibits more than a two-orders-of-magnitude increased Raman enhancement, hereby showing that with improved fabrication techniques it may be possible to approach the theoretical limit of SERS,[12] which has hitherto proven illusive. Conversely, imposing strict fabrication limitations results in an optimized design resembling the well-known bowtie-antenna design,[13] and unsurprisingly we observe similar experimental SERS enhancements.

Surface-enhanced Raman scattering (SERS) capitalizes on the local electromagnetic field enhancement near plasmonic metal nanostructures [4–11] to dramatically boost Raman scattering from molecules,

enabling detection sensitivity down to the single molecule level.[8,11,14–16] However, such giant enhancement is only found in structures with extremely fine feature size not compatible with standard lithographic fabrication.[16–19] In this paper, we applied topology optimization with realistic fabrication constraints to engineer metal nanostructures and experimentally demonstrated the SERS enhancement factor (EF) of 5×10^4 based on topology-optimized designs. While this EF is less than those reported in several previous works,[18,20] it is achieved using direct lithographic patterning with a specified resolution limit of 20 nm, and no post-lithography process is implemented to reduce the feature size. Our results, therefore, demonstrate a practical route for SERS substrate fabrication using standard lithographic fabrication tools to improve both processing yield and reproducibility.

Density-based topology optimization (TopOpt)[1,21] is a well-established numerical inverse-design method for creating highly optimized freeform solutions to structural-design problems, applicable across a wide range of physical systems,[2,22–25] where fabrication restrictions can be accounted for in the design process, e.g., by introducing minimum length-scales on the material phases.[26,27] When applying TopOpt, the physics is (most often) modeled using partial

differential equations. The design problem is recast as a constrained continuous-optimization problem, which is solved efficiently using a gradient-based optimization algorithm, allowing for a vast design space with nearly unlimited design freedom.[23] Recently, interest in applying TopOpt for photonics and plasmonics has grown[28,29] with recent applications to optimize a nanophotonic demultiplexer,[30] metasurface optics,[31–34] plasmonic nano-antennas,[35] plasmonic enhancement of thermal emission,[36] and topological photonics[21] to name a few. The ability of TopOpt to handle a vast design space is critical to the optimization of complex nanostructures, which is essential to approach the Raman enhancement limit.[3,12,37] While our prior work demonstrated how TopOpt can be used to design plasmonic nanoparticles with orders of magnitude greater enhancement than the standard bowtie antenna,[3] the investigation focused on two dimensional (2D) structures and, thus, practical fabrication limitations were not accounted for. Here, we extend our approach to complex 3D structures with full consideration of fabrication-related non-idealities such as limited feature sizes, non-vertical sidewall angles, and corner rounding.

First, we design a periodic array of three-dimensional metallic nanostructures made of platinum (Pt), resting on a blanket Pt film in an air background, starting from the initial material configuration of an empty air region above the Pt film, demonstrating the ability of TopOpt to identify a locally optimal structure from an empty design region. The goal of the design procedure is to tailor a structure in the periodic unit cell and to maximize the emission enhancement from a Raman molecule at a fixed point in space and at a set of targeted wavelengths (λ). To achieve this goal, we employ density-based topology optimization as detailed in our previous work.[3] Pt was chosen in this work since we found it to exhibit the largest enhancement.[3] In brief, the design procedure assumes a fixed position of the Raman molecule, modeled as coupled dipole absorption and emission processes. We model the physics as a two-step process using Maxwell's equations for

a time-harmonic electromagnetic field. First, the molecule is excited by an external source (at $\lambda = 532$ nm), followed by subsequent Raman emission of light from the molecule (at $\lambda = 549$ nm). The design domain consists of a brick-shaped spatial region with lateral dimensions 600×600 nm^2 (equal to the lateral periodicity) and a height of 200 nm, which is discretized using a structured mesh. The lateral dimensions of the design domain were chosen to limit the effect of electron backscattering in the EBL process but were not otherwise optimized. The design is formed iteratively, by gradually changing the material distribution in each element of the mesh to either contain platinum or air, in order to maximize the Raman enhancement, while simultaneously respecting the constraints imposed on the model problem. In the present study, we enforce an out-of-plane slant-angle on the design (incurred in the fabrication process) by employing a modified version of a filter and threshold procedure[26] as well as a minimum feature size of 20 nm (defined by the lithographic resolution) using a geometric length-scale constraint.[27] Details regarding the out-of-plane slant-angle constraint and the design process are found in Sec. A1 in the supplementary material.

The optimized nanostructure is depicted in Fig. 1. The black color indicates the Pt substrate, while the white color represents the optimized Pt nanostructures. Figure 1(a) presents a top-view of 3×3 unit cells for the optimized nanostructure, and Fig. 1(c) shows a tilted view of the same structure. Even though we started the design process with a uniform Pt layer as an initial guess, the optimization led to a structure with a narrow gap in between a pair of bowtie-like nano-antennas. This optimized design geometry is consistent with the common notion that nano-gaps strongly localize the electromagnetic field,[8–11] due to excitation of a localized plasmonic resonance combined with the corner singularity in the electric field near sharp tips,[14–16] a phenomenon which appears instrumental to large Raman enhancement. Scanning electron microscopy (SEM) images in
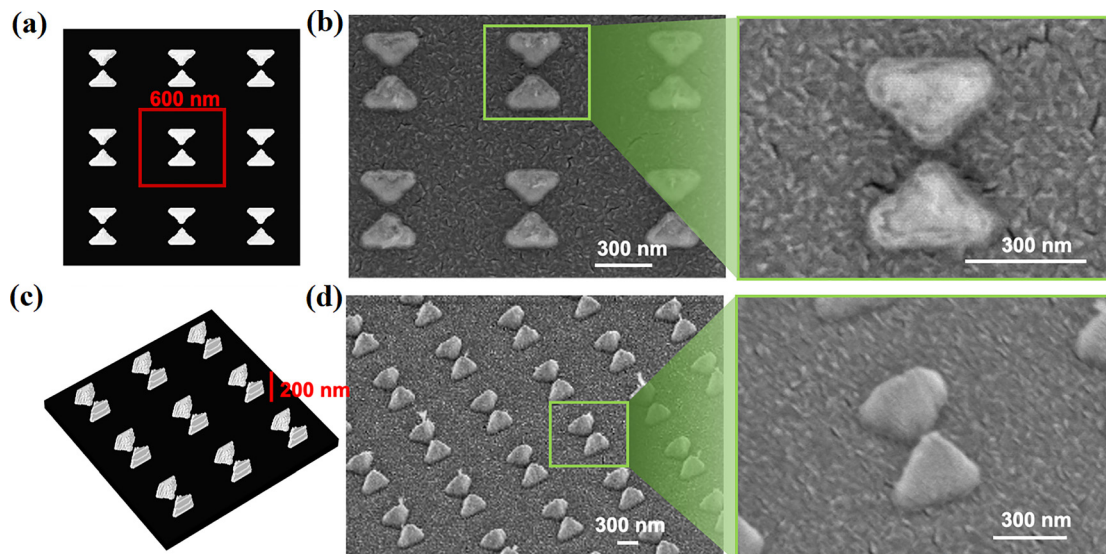
FIG. 1. Images of the periodic array of the optimized nanostructures with the unit cell having a lateral dimensions of 600×600 nm^2 and a metal thickness of 200 nm. (a) Top view of the optimized nanostructures and (b) scanning electron microscopy (SEM) image of the fabricated nanostructures. (c) and (d) Tilted-view of the structures in (a) and (b). The insets on the right in (b) and (d) show zoomed in views of the structures. Regions with silver color represent the optimized platinum nanostructure, and regions with black color indicate the platinum substrate in (a) and (c). The scale bar is 600in (a), 200in (c), and 300 nm in (b) and (d).

Figs. 1(b) and 1(d) illustrate the excellent fidelity of the nanostructures fabricated via a metal liftoff method, consistent with our design. An image comparison between the design mask file and a SEM image of the device shows more than 90% agreement between them, in terms of the number of identical pixels after elimination of noise with only few nm sized discrepancies along the particle edge. (Details of the calculation can be found in Sec. A3 in the supplementary material.)

To experimentally investigate the Raman enhancement, Rhodamine 6G (R6G, Sigma-Aldrich) was chosen as the model molecule, whose Raman scattering response has been investigated in multiple prior studies.[38–42] R6G with a concentration of 10^{-3} M was prepared by dissolving 47.5 mg of R6G powder into 100 ml of deionized (DI) water. Aqueous R6G solution with other concentrations are obtained by serial dilution of the initial solution in DI water. To transfer the R6G molecules onto the substrate, the platinum substrates were immersed in R6G solutions of varying concentrations for one hour and subsequently dried with nitrogen gas.

Raman spectra of R6G molecules on the substrates were measured using a Raman microscope (LabRam HR, HORIBA). Linearly polarized laser light at a wavelength of 532 nm was focused onto the substrate surface using a $50\times$ objective lens. Backscattered light was collected by the same objective lens and directed to a spectrometer with 1800-g/mm grating. The laser spot size was approximately 1 μm, while the area containing the fabricated nano-structure array was 30×30 μm^2. The total power incident on the sample surface was 37 ± 1 mW, measured at the sample holder stage. Data were collected at multiple locations for statistical averaging with an accumulation time of 1 s for all measurements.

Figures 2(a) and 2(b) show the Raman spectra of R6G measured on the optimized SERS substrate and a bare Si substrate as a reference. The R6G was incubated at concentrations of 10^{-5} M (SERS) and 10^{-2} M (Si), respectively. The Raman spectrum in Fig. 2(a) features intense peaks at 604, 761, 1172, 1303, 1356, and 1647 cm^{-1}, which correspond to main vibrational features of carbon skeleton stretching modes in the R6G molecule.[38,39,41,42] The strongest band is seen at 604 cm^{-1}, whose intensity was targeted for maximization in the design process. This band is assigned to an in-plane bending mode of the xanthene ring.[43]

To evaluate the experimental SERS enhancement factor (EF), we compare the Raman signal measured on the nano-structured substrates with that from the reference silicon substrate. The silicon substrate was used here due to its low (atomic-level) surface roughness compared to the nm-level roughness of a platinum film, which is difficult to capture accurately in simulations. The EF is determined using the following equation:

$$EF = \frac{I_{SERS}}{C_{SERS}} \times \frac{C_0}{I_0},$$

where I_{SERS} and I_0 are the intensities of the 604 cm^{-1} Raman peak measured on the SERS substrate and reference, respectively, and C_{SERS} and C_0 are the concentrations of R6G in the aqueous solution that the SERS and reference substrates were treated with Refs. 8, 14, and 42. Using the formula, we obtained an average SERS EF of $5 \pm 0.3 \times 10^4$ for the 604 cm^{-1} Raman peak. The measured EF is higher than that the EF-value of approximately 1075 predicted in our numerical simulations. The enhancement factor calculated from the numerical simulations is computed as the integral of the power, emitted through a halfplane above the substrate, for a single molecule placed on the optimized structure at the targeted spatial point, relative to the total power emitted through said halfplane by a single molecule placed on the reference silicon substrate, when illuminated by a plane wave at normal incidence. For reference, the experimentally measured Raman spectra of R6G on the pure Pt substrate is provided in Sec. A4 of the supplementary material. The observed mismatch between the experiment and simulation is likely due to the intrinsic roughness of the deposited Pt metal, which provides additional Raman signal amplification.

To demonstrate that the optimized nanostructure is robust against shape deviations and simultaneously compare the results to a well-known SERS geometry, we fabricated a parametrized reference bowtie structure [Figs. 3(d) and 3(e)], whose shape follows the contour of the topology optimized structure [Figs. 3(a) and 3(b)], as shown in Fig. 3. The Raman counts for Figs. 3(c) and 3(f) are both around 150 ± 7 by averaging nine spots on each substrate. The average enhancement factor is $5 \pm 0.3 \times 104$ for the 604 cm^{-1} Raman peak. Experimental results in Figs. 3(c) and 3(f) suggest that the SERS EF does not vary significantly between the two realizations, when accounting for the measurement errors (less than 15%).

Finally, we demonstrate numerically that TopOpt can be used to design nanostructures with significantly higher Raman enhancement
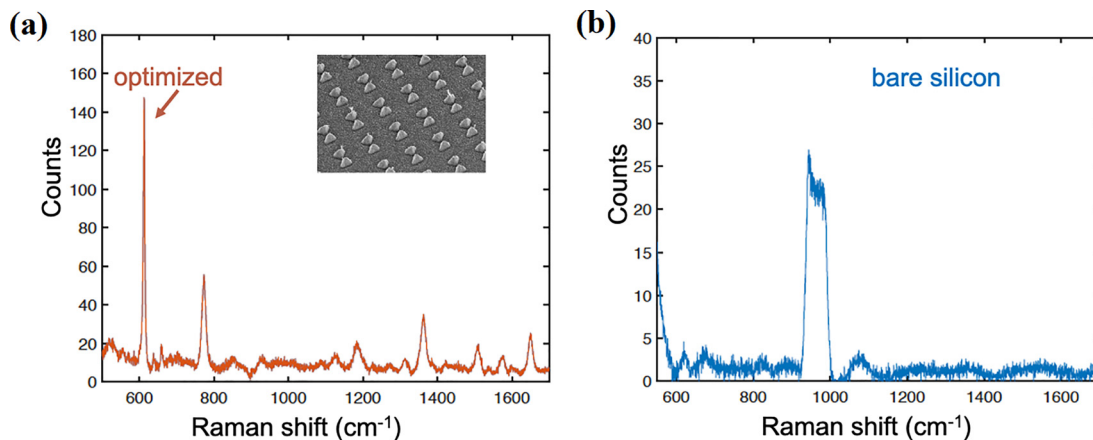
FIG. 2. Comparison of Raman-spectra of R6G molecules on topology optimized (a) Pt nanostructures and (b) silicon substrate. The background was subtracted.
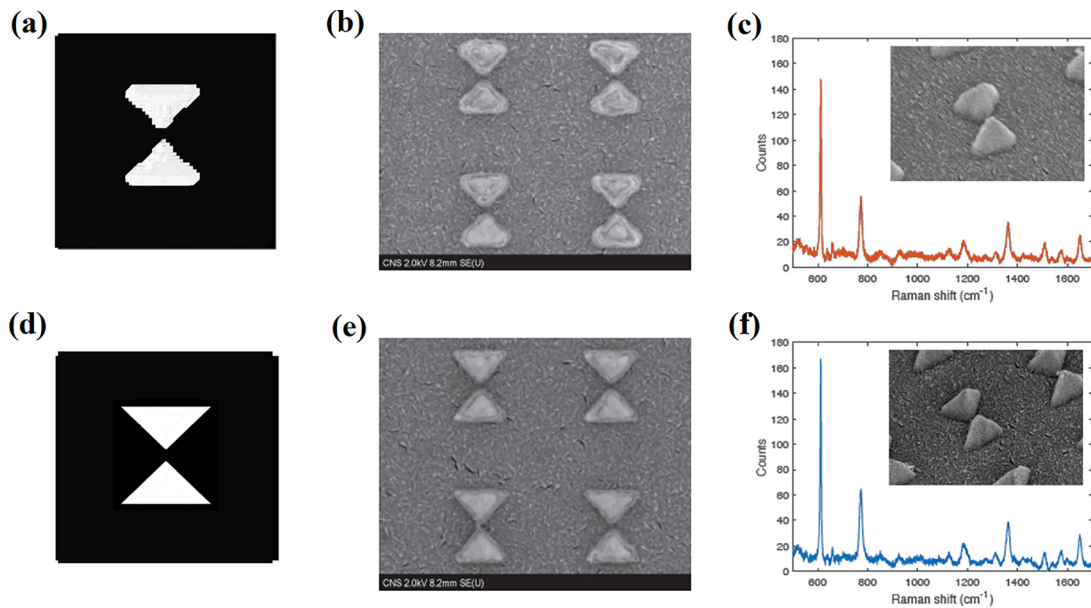
FIG. 3. Nanostructure geometries and SERS EF measurement results for the topology optimized structure and a parametrized triangular bowtie nanostructure. (a) The optimized nanostructure unit cell, (b) SEM of the fabricated nanostructure array, and (c) the measured Raman signal from the optimized nanostructure array in (b). (d)–(f) The corresponding information for the triangular bowtie nanostructures.

than that achieved by the nanostructure studied in Figs. 1–3. To this end, we relax the minimum-feature-size constraint from 20 to 5 nm. Furthermore, we reduce the lateral unit-cell area to $200 \times 200 \, \text{nm}^2$ and increase the unit-cell height to 300 nm, hereby increasing the density of the Raman enhancement points by a factor of 9, as well as increasing the design freedom in the out-of-plane direction. Making these adjustments, we design the Pt nanostructure shown in Fig. 4. Figures 4(a)–4(c) present a tilted view, a top-down view, and a cross-sectional view, respectively. The footprint of the designable unit cell is highlighted in Fig. 4(b) using a red box, and the position of the Raman molecule is denoted by a red dot. The optimized nanostructure

resembles an amalgamation of an in-plane bowtie-like antenna and an out-of-plane horn-like structure, suggesting that a combination of these two feature types may be exploited to increase the EF for other SERS structures. Figure 4(d) shows the nanostructure with a saturated colorscheme presenting the magnitude of the emitted power, $|\mathbf{P}|$, shown in two vertical planes, for an array of Raman molecules placed at the point targeted for Raman enhancement maximization. Finally, Fig. 4(e) presents a map of the achieved EF when placing a single molecule at different positions in the unit-cell, max-normalized to a molecule situated at the position targeted in the optimization process, in the (x,z)-plane at y = 0 in a single unit-cell. From the figure, it is seen
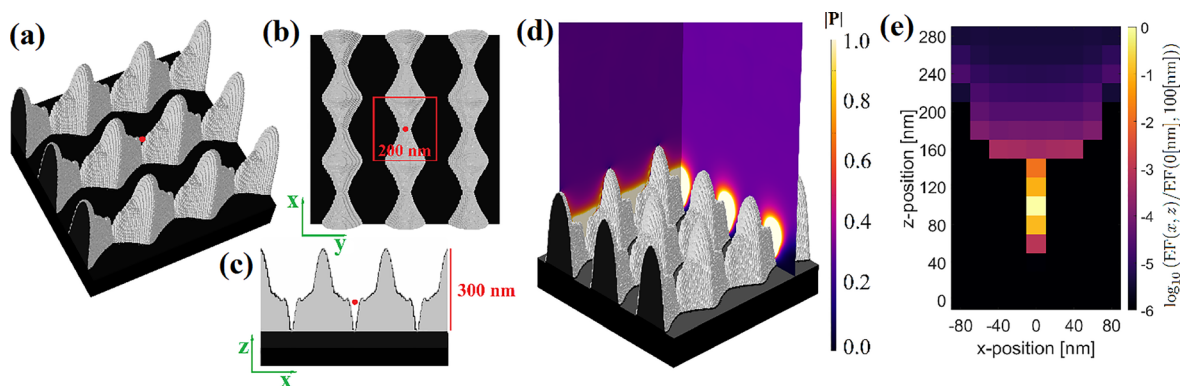
FIG. 4. SERS nanostructure designed using TopOpt with relaxed fabrication limitations. (a) Tilted-view of the optimized nanostructure. (b) Top-down view of the nanostructure. (c) (x,z)-plane cross-sectional view of the nanostructure containing the position of the Raman molecule. (d) Magnitude of the power flow, $|\mathbf{P}|$, shown in two vertical planes and saturated at $|\mathbf{P}| = 1$, emitted by Raman molecules placed at the point(s) targeted for Raman enhancement maximization when illuminated by 532 nm light at normal incidence. (e) Map of the enhancement factor (EF) in the unit-cell at y = 0 for a molecule placed at different (x,z)-positions, max-normalized to the EF at the targeted molecule position.

that as the molecule is shifted more than 20 nm from the target position, the EF drops by several orders of magnitude, illustrating that the optimized design has indeed been tailored for a specific molecule position, as specified in the inverse design problem formulation. For the design in Fig. 4, the numerically calculated enhancement factor relative to the Raman molecule placed on a smooth silicon surface is approximately 531 000. This is an increase by more than two orders of magnitude (compared to the EF of approximately 1075 for the previous design) and within a factor of 10 of the surface-scaling SERS enhancement bound of $\approx 3.433 \times 10^6$ (estimated for the given unit-cell dimensions using Ref. 12).

In this work, we demonstrated the experimental implementation of nanostructure arrays, designed via topology optimization, to maximize surface-enhanced Raman scattering. Our optimization approach incorporates approximations of practical fabrication constraints to generate realistic designs commensurate with direct lithographic patterning, which yields high EF values as validated in our experiment. These results illustrate the practical applicability and potential of applying TopOpt to Raman and other scattering problems to produce designs suitable for scalable manufacturing. Furthermore, we demonstrated that TopOpt may be used to design nanostructures exhibiting even higher EFs by relaxing the fabrication constraints, motivating a hunt for improved fabrication techniques. It is worth noting, that if one selected different unit-cell dimensions for the periodic SERS design problem considered in this work, it may be possible to design structures that outperform the triangular bowtie used as a reference in this work. However, as the goal of this work is to demonstrate the feasibility of the proposed method as a tool to design directly manufacturable SERS nanostructures, a study of the maximally attainable performance using the specified fabrication constraints is left for future works.

While traditional design techniques based on analytical models and intuition are able to solve relatively simple problems, such as designing SERS metasurfaces (e.g., by tailoring a bowtie-antenna array), our TopOpt-based method allows for envisioning and solving significantly more challenging design problems. For example, one can design of nanostructures tailored for maximizing Raman enhancement in a geometrically complex in-plane device, where analytical models and standard intuition cannot easily address the simultaneous objectives of emission enhancement and waveguide coupling.[3,44,45] More generally, the density-based topology optimization method offers a systematic approach for identifying high performance solutions to challenging design problems that balance multiple physical processes, enabling the creation of complex devices. Finally, while this work considers a single Raman molecule at a fixed point in space and optimizes the emission from said particle, our ultimate goal is the computationally much more challenging problem of optimizing the average response for a large ensemble of molecules situated at different locations in space. Solving that problem may lead to very different and superior structures, which is the subject of ongoing and future works.

See the supplementary material for four appendixes that provide descriptions of the inverse design process (A1), the substrate nanofabrication (A2), a comparison of the designed and fabricated Pt nanostructure footprint (A3), and the Raman spectra of R6G on a Pt substrate (A4).

DATA AVAILABILITY

The data that support the findings of this study are available from the corresponding author upon reasonable request.

REFERENCES

[1]M. P. Bendsøe and O. Sigmund, *Topology Optimization: Theory, Methods and Applications* (Springer, 2003).

[2]J. Alexandersen and C. S. Andreasen, "A review of topology optimisation for fluid-based problems," Fluids **5**, 29 (2020).

[3]R. E. Christiansen, J. Michon, M. Benzaouia, O. Sigmundand, and S. G. Johnson, "Inverse design of nanoparticles for enhanced Raman scattering," Opt. Express **28**, 4444 (2020).

[4]I. Mrozek and A. Otto, "Surface enhanced Raman scattering," J. Phys.: Condens. Matter **4**, 1143 (1992).

[5]K. Kneipp, Y. Wang, H. Kneipp *et al.*, "Single molecule detection using surface-enhanced raman scattering (SERS)," Phys. Rev. Lett. **78**, 1667 (1997).

[6]S. Nie and S. R. Emory, "Probing single molecules and single nanoparticles by surface-enhanced Raman scattering," Science **275**, 1102–1106 (1997).

[7]K. Kneipp, H. Kneipp, I. Itzkan, R. R. Dasari, and M. S. Feld, "Surface-enhanced Raman scattering and biophysics," J. Phys.: Condens. Matter **14**, R597 (2002).

[8]E. C. L. Ru, E. Blackie, M. Meyer, and P. G. Etchegoint, "Surface enhanced Raman scattering enhancement factors: A comprehensive study," J. Phys. Chem. C **111**, 13794–13803 (2007).

[9]M. J. Banholzer, J. E. Millstone, L. Qin, and C. A. Mirkin, "Rationally designed nanostructures for surface-enhanced Raman spectroscopy," Chem. Soc. Rev. **37**, 885–897 (2008).

[10]E. C. L. Ru and P. G. Etchegoin, *Principles of Surface-Enhanced Raman Spectroscopy: And Related Plasmonic Effects* (Elsevier, 2009).

[11]W. Zhu, M. G. Banaee, D. Wang, Y. Chu, and K. B. Crozier, "Lithographically fabricated optical antennas with gaps well below 10 nm," Small **7**, 1761–1766 (2011).

[12]J. Michon, M. Benzaouia, W. Yao, O. D. Miller, and S. G. Johnson, "Limits to surface-enhanced Raman scattering near arbitrary-shape scatterers," Opt. Express **27**, 35189 (2019).

[13]N. A. Hatab, C. Hsueh, A. L. Gaddis *et al.*, "Free-standing optical gold bowtie nanoantenna with variable gap size for enhanced Raman spectroscopy," Nano Lett. **10**, 4952–4955 (2010).

[14]K. Li, Y. Wang, K. Jiang *et al.*, "Free-standing Ag triangle arrays a configurable vertical gap for surface enhanced Raman spectroscopy," Nanotechnology **28**, 385401 (2017).

[15]J. D. Caldwell, O. Glembocki, F. J. Bezares *et al.*, "Plasmonic nanopillar arrays for large-area, high-enhancement surface-enhanced Raman scattering sensors," ACS Nano **5**, 4046–4055 (2011).

[16]T. Gong, Y. Luo, C. Zhao *et al.*, "Highly reproducible and stable surface-enhanced Raman scattering substrates of graphene-Ag nanohole arrays fabricated by sub-diffraction plasmonic lithography," OSA Continuum **2**, 582 (2019).

[17]L. Surbhi, L. Stephan, and J. H. Naomi, "Nano-optics from sensing to waveguiding," Nat. Photonics **1**, 641–648 (2007).

[18]D. R. Ward, N. K. Grady, C. S. Levin *et al.*, "Electromigrated nanoscale gaps for surface-enhanced Raman spectroscopy," Nano Lett. **7**, 1396–1400 (2007).

[19]C. M. Gruber, L. O. Herrmann, A. Olziersky et al., "Fabrication of bow-tie antennas with mechanically tunable gap sizes below 5 nm for single-molecule emission and Raman scattering," in *15th International Conference on Nanotechnology (IEEE-NANO 2015)* (IEEE, 2015), pp. 20–24.

[20]A. Gopinath, S. V. Boriskina, W. R. Premasiri et al., "Plasmonic nanogalaxies: Multiscale aperiodic arrays for surface-enhanced Raman sensing," Nano Lett. **9**, 3922–3929 (2009).

[21]R. E. Christiansen and O. Sigmund, "Inverse design in photonics by topology optimization: Tutorial," J. Opt. Soc. Am. B **38**(2), 496–509 (2021).

[22]R. E. Christiansen and E. Fernandez-Grande, "Design of passive directional acoustic devices using Topology Optimization—From method to experimental validation," J. Acoust. Soc. Am. **140**, 3862–3873 (2016).

[23]N. Aage, E. Andreassen, B. S. Lazarov, and O. Sigmund, "Giga-voxel computational morphogenesis for structural design," Nature **550**, 84–86 (2017).

[24]R. E. Christiansen, F. Wangand, and O. Sigmund, "Topological insulators by topology optimization," Phys. Rev. Lett. **122**, 234502 (2019).

[25]C. Lundgaard, K. Engelbrechtand, and O. Sigmund, "A density-based topology optimization methodology for thermal energy storage systems," Struct. Multidiscip. Optim. **60**, 2189–2204 (2019).

[26]F. Wang, B. S. Lazarov, and O. Sigmund, "On projection methods, convergence and robust formulations in topology optimization," Struct. Multidiscip. Optim. **43**, 767–784 (2011).

[27]M. Zhou, B. S. Lazarov, F. Wang, and O. Sigmund, "Minimum length scale in topology optimization by geometric constraints," Comput. Methods Appl. Mech. Eng. **293**, 266–282 (2015).

[28]J. S. Jensen and O. Sigmund, "Topology optimization for nano-photonics," Laser Photonics Rev. **5**, 308–321 (2011).

[29]S. Molesky, Z. Lin, A. Y. Piggott et al., "Inverse design in nanophotonics," Nat. Photonics **12**, 659–670 (2018).

[30]A. Y. Piggott, J. Lu, K. G. Lagoudakis et al., "Inverse design and demonstration of a compact and broadband on-chip wavelength demultiplexer," Nat. Photonics **9**, 374–377 (2015).

[31]E. W. Wang, D. Sell, T. Phan, and J. A. Fan, "Robust design of topology-optimized metasurfaces," Opt. Mater. Express **9**, 469 (2019).

[32]S. D. Campbell, D. Sell, R. P. Jenkins et al., "Review of numerical optimization techniques for meta-device design [Invited]," Opt. Mater. Express **9**, 1842 (2019).

[33]M. Y. Shalaginov, S. D. Campbell, S. An et al., "Design for quality: Reconfigurable flat optics based on active metasurfaces," Nanophotonics **9**, 3505–3534 (2020).

[34]H. Chung and O. D. Miller, "High-NA achromatic metalenses by inverse design," Opt. Express **28**, 6945 (2020).

[35]E. Wadbro and C. Engström, "Topology and shape optimization of plasmonic nano-antennas," Comput. Methods Appl. Mech. Eng. **293**, 155–169 (2015).

[36]Z. A. Kudyshev, A. V. Kildishev, V. M. Shalaev, and A. Boltasseva, "Machine-learning-assisted metasurface design for high-efficiency thermal emitter optimization," Appl. Phys. Rev. **7**, 021407 (2020).

[37]O. D. Miller, A. G. Polimeridis, M. T. H. Reid et al., "Fundamental limits to optical response in absorptive systems," Opt. Express **24**, 3329 (2016).

[38]P. Hildebrandt and M. Stockhurger, "Surface-enhanced resonance Raman spectroscopy of rhodamine 6G adsorbed on colloidal silver," J. Phys. Chem. **88**, 5935–5944 (1984).

[39]S. Shim, C. M. Stuart, and R. A. Mathies, "Resonance Raman cross-sections and vibronic analysis of rhodamine 6G from broadband stimulated Raman spectroscopy," ChemPhysChem **9**, 697–699 (2008).

[40]A. M. Michaels, M. Nirmal, and L. E. Brus, "Surface enhanced Raman spectroscopy of individual rhodamine 6G molecules on large Ag nanocrystals," J. Am. Chem. Soc. **121**, 9932–9939 (1999).

[41]A. Kudelski, "Raman studies of rhodamine 6G and crystal violet sub-monolayers on electrochemically roughened silver substrates: Do dye molecules adsorb preferentially on highly SERS-active sites?," Chem. Phys. Lett. **414**, 271–275 (2005).

[42]P. Zhang, S. Yang, L. Wang et al., "Large-scale uniform Au nanodisk arrays fabricated via x-ray interference lithography for reproducible and sensitive SERS substrate," Nanotechnology **25**, 245301 (2014).

[43]H. Watanabe, N. Hayazawa, Y. Inouye, and S. Kawata, "DFT vibrational calculations of rhodamine 6G adsorbed on silver: Analysis of tip-enhanced raman spectroscopy," J. Phys. Chem. B **109**, 5012–5020 (2005).

[44]X. Wang, S. C. Huang, S. Hu, S. Yan, and B. Ren, "Fundamental understanding and applications of plasmon-enhanced Raman spectroscopy," Nat. Rev. Phys. **2**, 253–271 (2020).

[45]D. M. Kita, J. Michon, and J. Hu, "A packaged, fiber-coupled waveguide-enhanced Raman spectroscopic sensor," Opt. Express **28**, 14963 (2020).

A1 - Inverse design of SERS substrate using Topology Optimization

The design domain for the topology-optimized nanostructure array in Figs. 1-3 is a unit cell with a lateral dimension of 600 nm × 600 nm and a height of 200 nm discretized using a uniform mesh with an element side length of 5 nm. For the array in Fig. 4 the unit cell has lateral dimensions of 200 nm × 200 nm and a height of 300 nm with an element side length of 2 nm.

The electromagnetic simulation is performed in COMSOL Multiphysics[46] using first-order finite elements. The optimization problem is solved using the Globally Convergent Method of Moving Asymptotes (GCMMA)[47]. For the physics modeling, the Raman molecule is modeled as a point dipole absorber/emitter at the center gap location. The wavelength of the incident field is 532 nm, while the wavelength of the emitted field is 549 nm. The emitted power, due to Raman scattering from the molecule, is calculated using an array-scanning method[3], which allows us to model incoherent dipole emission using a set of computations with Bloch-periodic boundary conditions. The relative permittivity of Pt is obtained from ellipsometry data measured on a J.A. Woollam M-88 multi-wavelength ellipsometer.

In the optimization process the Pt material distribution in the design domain is controlled using a two dimensional design field, $\xi(x,y)$, determining the cross-section of the Pt material layout. The design field is subjected to a smoothing scheme[26] using a standard cone-shaped filter and a filter radius of $r_f = 40$ nm, resulting in the filtered field $\tilde{\xi}(x,y)$. Following the smoothing operation, the design field is subjected to a height-dependent thresholding operation,

$$T\big(\tilde{\xi}(x,y),\eta(z),\beta\big) = \frac{tanh(\beta \cdot \eta(z)) + tanh\left(\beta \cdot \left(\tilde{\xi}(x,y) - \eta(z)\right)\right)}{tanh(\beta \cdot \eta(z)) + tanh(\beta \cdot (1 - \eta(z)))},$$

With a thresholding sharpness β and thresholding level $\eta(z)$. This operation creates an extruded three-dimensional Pt-material layout (approximately) respecting the desired out-of-plane minimum side-wall slant-angle. This angle is specified via an interplay between the filter radius r_f and the heigh-dependent thresholding level,

$$\eta(z) = \eta_1 + \left(\frac{(z - z_1)}{(z_2 - z_1)}\right) \cdot (\eta_2 - \eta_1).$$

Here $\eta_1 < \eta_2 \in [0,1]$ and $z_1(z_2)$ denotes the z-coordinate at the bottom(top) of the design domain.

In order to allow design freedom at the start of the optimization process and ensure a final (near) binary material distribution, the thresholding strength is increased gradually in the optimization process using the values, $\beta = \{8, 16, 32\}$.

As a final step, the filtered and thresholded design field is introduced into the model of the physics by using it to interpolate the relative permittivity in the design domain[48].

After the optimization process is complete the optimized permittivity distribution is sampled at the base of the design domain in (x,y)-coordinates with 0.5 nm resolution. The sampled field is smoothed with a 1.5 nm filter radius to eliminate kinks and the 50%-level contour extracted and used as the blueprint for fabrication.

A2 - Nanofabrication of the substrate

Platinum is initially deposited on the top of a silicon substrate using an electron beam evaporation system at a rate of 0.1 nm/s. The thickness of this Pt layer is 200 nm, which is sufficient to prevent interaction of the light with the underlying Si substrate. Then a layer of ZEP520A resist was spin coated (500 rpm, 5 s; 3000 rpm, 60 s) onto the substrate. Electron beam lithography (Elionix F-125) was used to define the structure. After exposure, the sample was developed in O-xylene for 2 min. The resulting pattern served as lift-off mask during subsequent metallic platinum evaporation step. A thin layer of titanium/platinum was deposited by electron beam evaporation and the thickness (10/200 nm) were confirmed by profilometer. The sample was immersed in acetone overnight to remove the resist, thereby forming platinum metallic structures on the substrate. The samples were cleaned by extensive rinsing in acetone and isopropyl before nitrogen gun drying.

A3 - Design and fabricated Pt nanostructure

In order to investigate the correspondence between the nominal blueprint design and the fabricated structure, a SEM images was first turned to black and white image in a 0-255 gray scale by setting an appropriate threshold of 100; any position with gray scale below 100 turns to black and the remaining part turns to white. Then the figure is zoomed so that it has maximum overlap with design file. The designed file and the SEM image are shown in Fig. S1a-b. Finally, the differences of these two figures are plotted as the black areas in Fig. S1c with the surrounding noise eliminated. Denoting black areas in Fig. S1a and Fig. S1c as S_1 and S_2, the percentage of agreement is defined as $1 - \frac{S_2}{S_1}$, which was calculated as around 90%.
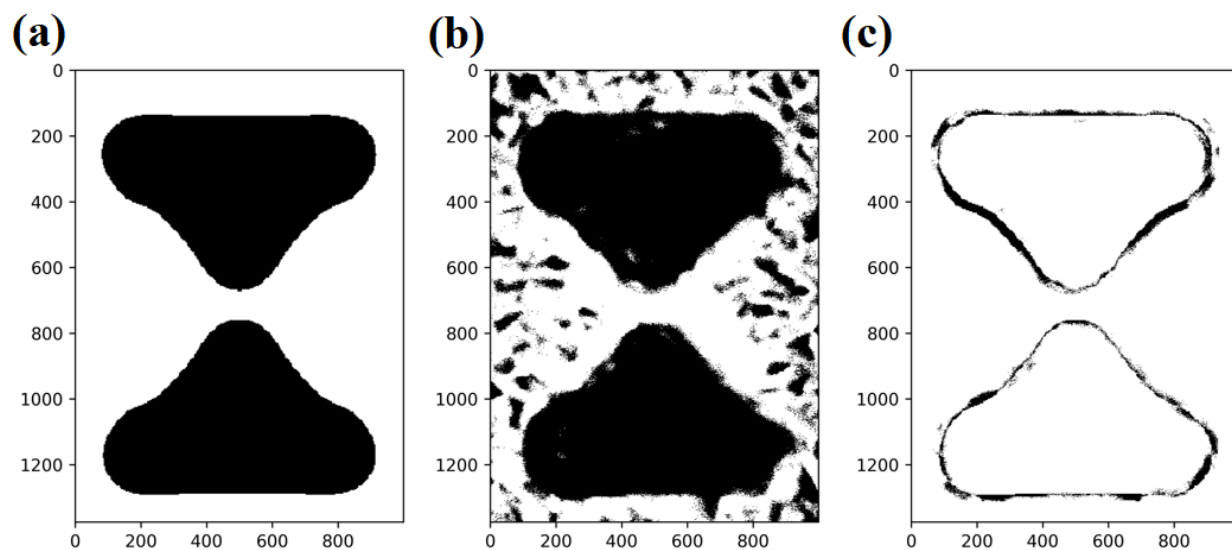
Figure S1. (a) the optimized design file, the x and y axis denote pixel number. (b) Black and white SEM image (Fig. 1b in the main text). (3) Difference (black areas) between the design file and SEM image.

A4 - Raman spectra of R6G on the Pt substrate

Figures S2a-b show the Raman spectra of R6G measured on the optimized SERS substrate and a pure Pt substrate as a reference. The R6G was incubated at concentrations of 10^{-5} M for both substrate. The average enhancement factor of optimized Pt nanostructure is 10 times higher than that of pure Pt substrate.
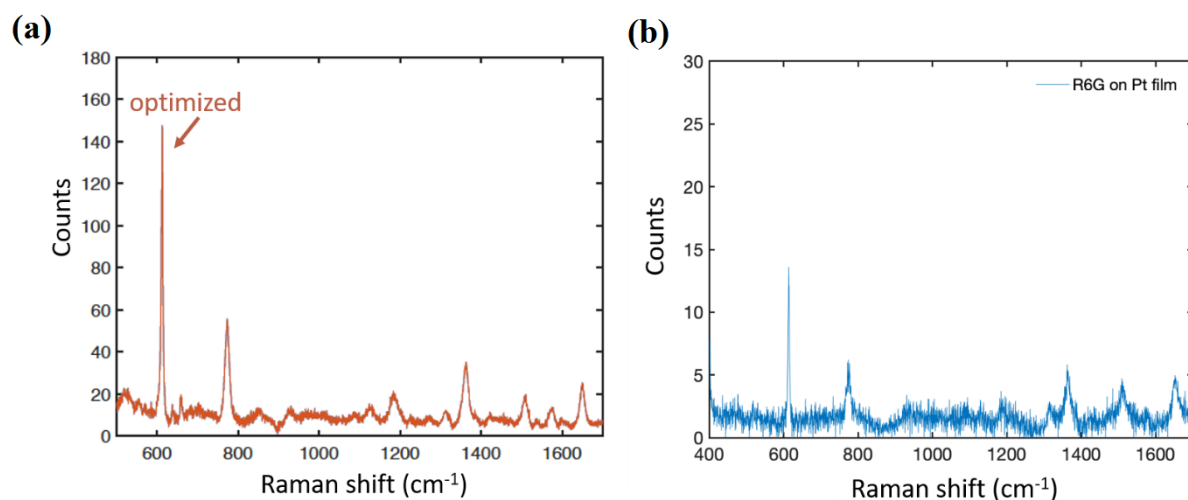
Figure S2. Comparison of Raman-spectra of R6G molecules on topology optimized (a) Pt nanostructures and (b) pure Pt substrate. The background was subtracted.

References:

3.   R.E. Christiansen, J. Michon, M. Benzaouia, O. Sigmundand S. G. Johnson Inverse design of nanoparticles for enhanced Raman scattering. *Optics Express* **28**, 4444 (2020).

26.   F. Wang, B. S. Lazarov and O. Sigmund. On projection methods, convergence and robust formulations in topology optimization. *Structural and Multidisciplinary Optimization* **43**, 767–784 (2011).

46.   COMSOL Multiphysics v. 5.5,.

47.   K. Svanberg. A Class of Globally Convergent Optimization Methods Based on Conservative Convex Separable Approximations. *SIAM Journal on Optimization* **12**, 555–573 (2002).

48.   R. E. Christiansen, J. Vester-Petersen, S. P. Madsen, and O. Sigmund. A non-linear material interpolation for design of metallic nano-particles using topology optimization. *Computer Methods in Applied Mechanics and Engineering* **343**, 23–39 (2019).